Hindawi
Mathematical Problems in Engineering
Volume 2021, Article ID 9947090, 11 pages
https://doi.org/10.1155/2021/9947090

Research Article

Behavior Analysis of a Flexure Hinge Array

Ngoc Le Chau,[1] Ngoc Thoai Tran,[1] and Thanh-Phong Dao [2,3]

[1]*Faculty of Mechanical Engineering, Industrial University of Ho Chi Minh City, Ho Chi Minh City, Vietnam*
[2]*Division of Computational Mechatronics, Institute for Computational Science, Ton Duc Thang University, Ho Chi Minh City, Vietnam*
[3]*Faculty of Electrical & Electronics Engineering, Ton Duc Thang University, Ho Chi Minh City, Vietnam*

Correspondence should be addressed to Thanh-Phong Dao; daothanhphong@tdtu.edu.vn

Received 5 March 2021; Revised 30 March 2021; Accepted 1 April 2021; Published 14 April 2021

Academic Editor: Dr. Dilbag Singh

Compliant mechanisms have been well designed to reach an ultra-high accuracy in positioning systems. However, the displacement of compliant mechanisms is still a major problem that restricts practical applications. Hence, a new flexure hinge array (FHA) is proposed to improve its displacement in this article. This paper is aimed to design and optimize the FHA. The structure of FHA is constructed by series-parallel array. Analytical calculations of the FHA are derived so as to analyze the stiffness and deformation. The displacement of the FHA is optimized by moth-flame optimization algorithm. The results determined that optimal parameters are found at L_{t1} of 20.58 mm, w_{t1} of 1.92 mm, and w_{t2} of 2.29 mm. Besides, the optimal displacement is about 27.02 mm. Through Kruskal–Wallis test, the results verified that the proposed MFO outperforms other optimization algorithms in terms of searching the largest displacement. Validations of the analytical models are verified through simulations and experiments. The theoretical results are close to the experimental results. Additionally, the displacement of the FHA is superior that of existing joints. The displacement in the z-direction is approximately 32 mm according to a displacement of 12 mm in the x-direction.

1. Introduction

Compliant mechanism (CM) is a monolithic structure; its motion is a cause of elastic deformations of flexure hinge [1–3]. CMs are used to transfer motions, force, or energy being similar to kinematic joint-based mechanisms [4, 5]. Unlike traditional mechanisms, CMs can be monolithically manufactured from a material piece. Therefore, it can decrease assemble parts, needs no lubricant and free friction, and can reduce cost of manufacturing [6–10]. Practically, CMs are suitable candidates for applications in microdevices, precision instrument, microgripper, actuator, and manipulator [11–16]. It is well-known that there is a very close relationship between the CMs and lamina emergent mechanism (LEM) where the LEM is made by a sheet metal [17–20]. LEMs emerge out of sheet plane when they are subjected to a load [21]. It initializes from a flat state, and it is hence easy to storing, packing, and shipping.

LEMs also have advantages similar to CMs but it has a motion moving from fabrication plane [22]. So, it has some potential applications such as electronics, automobile, biomedical engineering, micro-electro mechanical systems, credit card of smartphone, and tablet and cellphone holder [17]. Therefore, LEMs are considered as compliant joints or flexure hinges. In the recent decades, a lot of researchers have suggested many types of hinges for LEMs [19, 21–24]. Particularly, LEMs well developed by benefitting of bistable advantages, foldable mechanism, and material strength [25–29]. However, the displacement of existing LETs and LEMs is still limited thanks to their designed structures. Furthermore, the bearing capacity of LETs and LEMs is still the major problem that can restrict engineering applications. On the other hand, the existing LETs are limited in the displacement and capacity of load bearing. In order to overcome the mentioned limitations, the present study suggests a new flexure hinge array (FHA) which can provide a large displacement range without static failures. Besides, the FHA can bear a large range of load.

In order to analyze the stiffness and displacement of LETs, several analytical methods are proposed, including

integral method, pseudorigid-body model [17, 30], compliance matrix [31, 32], and closed-form models [33, 34]. The pseudorigid-body model benefits of the traditional mechanism theory but its accuracy is affected by assigning positions of torsional springs. Meanwhile, the compliance matrix method is only suitable for simple structures. With the complex shape of the FHA, the pseudorigid-body model and compliance matrix method are difficult to be employed. Thereafter, the closed-form model, which is based on the beam theory and series-parallel system, is adopted for analyzing the FHA.

The goal of this article is to design and optimize a new FHA. The structure of FHA is constructed by using a leaf hinge array in series-parallel connection. Analytical models are formulated to analyze the stiffness and displacement of the FHA, and then, the displacement of the FHA is optimized by using moth-flame optimization algorithm [35]. The proposed optimization method is compared with other methods in terms of finding the largest displacement of the FHA. The theoretical models are then verified by simulations and experiments. The performances of the FHA are compared with other existing hinges.

The rest of this paper is arranged as follows: Section 2 presents about a conceptual design for the FHA. Analytical modeling for the FHA is given in Section 3. Results and discussion are presented in Section 4. Conclusions and future work are presented in Section 5.

2. Conceptual Design for Flexure Hinge Array

A conceptual design of the FHA is built by arranging three LET hinges in a series to bear a single load in a direction or combined loads in multiple directions. A LET hinge can recognize bending elements and torsional elements. In order to create the FHA, it initializes from a basic LET hinge which consists of four types of torsional elements 1, four types of torsional elements 2, and two types of bending elements 1, as illustrated in Figure 1(a). Besides, a shape of the torsional element 2 is designed by generating radius curves so as to increase a flexibility of the LET, and then, three LET hinges are connected together through the bending element 2 to generate a large displacement. Parameters of a basic LET are illustrated in Figures 1(a) and 1(b). The detailed parameters of the bending elements and the torsional elements are labeled, as given in Figure 1(b). Overall dimensions are provided in Table 1.

In order to generate a large displacement, three basic LETs are connected in series to make an array of flexure hinges, so-called FHA. Three TLET flexure hinges are combined through a bending element 3, as illustrated in Figure 2. Dimensions of the FHA are given as in Figure 2 and Table 1. The performances of both the suggested FHA are analyzed to evaluate the reliability during its working without failures. Theoretical equations for the FHA are provided, and then, validity of the analytical model is verified through simulations and experiments. In this study, L_{t1}, w_{t1}, and w_{t2} ($20.18\,\text{mm} \le L_{t1} \le 24.67\,\text{mm}$, $1.92\,\text{mm} \le w_{t1} \le 2.34\,\text{mm}$, $2.30\,\text{mm} \le w_{t2} \le 2.80\,\text{mm}$) are main design variables; meanwhile, other parameters are constant.

3. Modeling of Stiffness and Displacement

Analytical equations of the FHA are established to demonstrate the stiffness and displacement. From scheme of basic LETs (see in Figure 1(b)), an equivalent diagram of the basic LETs is illustrated (see in Figure 3).

Figure 4 gives an equivalent stiffness system of the basic LET.

The stiffness of the torsional segment is determined by

$$k_{\text{eqt}} = \frac{k_{t1} \times k_{t2}}{k_{t1} + k_{t2}}, \tag{1}$$

in which equivalent stiffness of torsional segment is $k$eqt, stiffness of torsion element 1 is kt1, and torsion element 2 is kt2.

Two springs of bending element 1 are in a parallel system. The equivalent stiffness of these two springs is computed as

$$k_{\text{eqb1}} = \frac{1}{2k_{b1}}, \tag{2}$$

in which k_{eqb1} is the equivalent stiffness of the parallel system, and k_{b1} is the stiffness of bending element 1.

The equivalent stiffness of bending element 2 is as follows:

$$k_{\text{eqb2}} = \frac{1}{2k_{b2}}, \tag{3}$$

where k_{eqb2} and k_{b2} are the equivalent stiffness and stiffness of bending element 2, respectively.

The bending stiffness of a basic LET (Figure 1(b)) is described by the following equation:

$$\frac{1}{K_{\text{eq-basic LET}}} = \frac{1}{k_{\text{eqt}}} + \frac{1}{k_{\text{eqb1}}} + \frac{1}{k_{\text{eqb2}}} + \frac{1}{k_{\text{eqt}}} + \frac{1}{k_{\text{eqb1}}} + \frac{1}{k_{\text{eqb2}}} + \frac{1}{k_{b3}}, \tag{4}$$

in which the bending elements are calculated by [23]

$$k_{b1} = \frac{Ew_{b1}t^3}{12L_{b1}^3}, \tag{5}$$

$$k_{b2} = \frac{Ew_{b2}t^3}{12L_{b2}^3}, \tag{6}$$

$$k_{b3} = \frac{Ew_{b3}t^3}{12L_{b3}^3}, \tag{7}$$

with Young's modulus is E and the thickness is t. Other dimensions such as (w_{b1}, L_{b1}), (w_{b2}, L_{b2}), and (w_{b3}, L_{b3}) are the width and length of bending element 1, bending element 2, and bending element 3, respectively.

The stiffness of torsion element 1 and torsion element 2 is as follows [23, 36]:

$$k_{t1} = w_{t1}t^3\frac{G}{L_{t1}}\left[\frac{1}{3} - 0.21\frac{t}{w_{t1}}\left(1 - \frac{t^4}{12w_{t1}^4}\right)\right], \tag{8}$$

$$k_{t2} = w_{t2}t^3\frac{G}{L_{t2}}\left[\frac{1}{3} - 0.21\frac{t}{w_{t2}}\left(1 - \frac{t^4}{12w_{t2}^4}\right)\right], \tag{9}$$

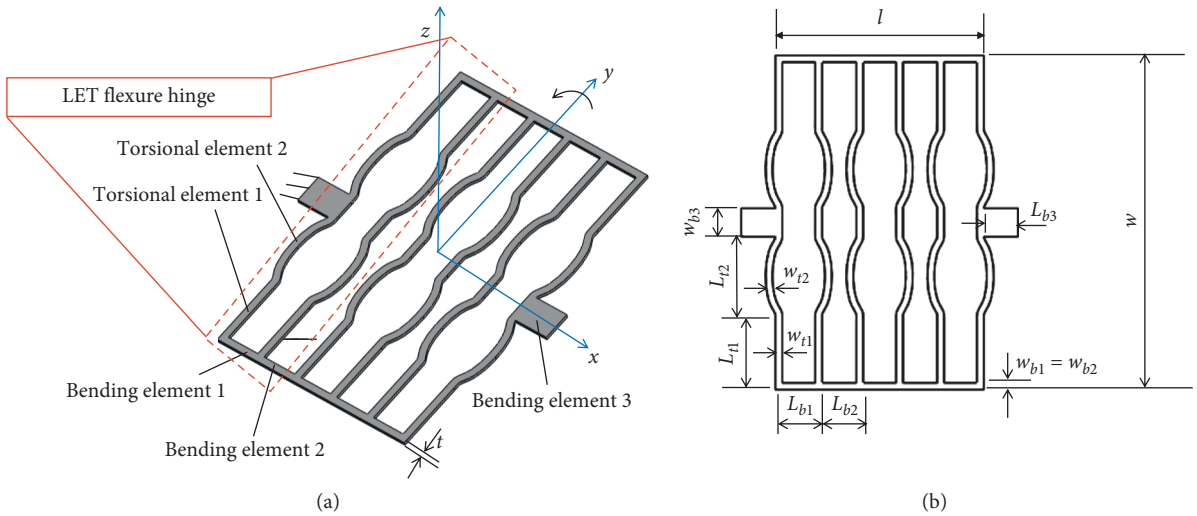

Figure 1: A basic LET: (a) 3D structure; (b) 2D dimensions.

Table 1: Dimensions of the FHA (unit: mm).

Symbol	L_{t1}	L_{t2}	L_{b1}	L_{b2}	L_{b3}	w_{b1}	w_{b2}	w_{b3}	w_{t1}
Value	Variable	23	13	13	10	2	2	8	Variable
Symbol	L	w	t	l	l_1	l_2	l_3	W	w_{t2}
Value	407	97	1	65	20	40	30	137	Variable

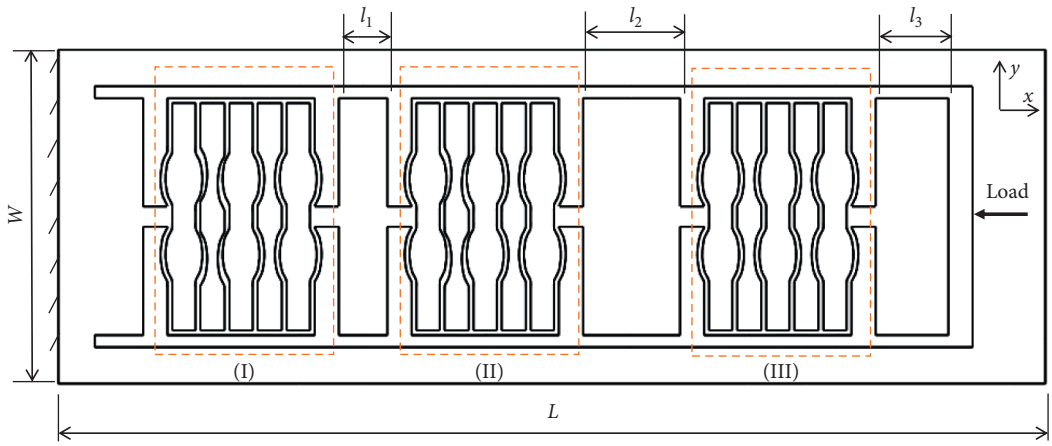

Figure 2: Model of the proposed flexure hinge array.

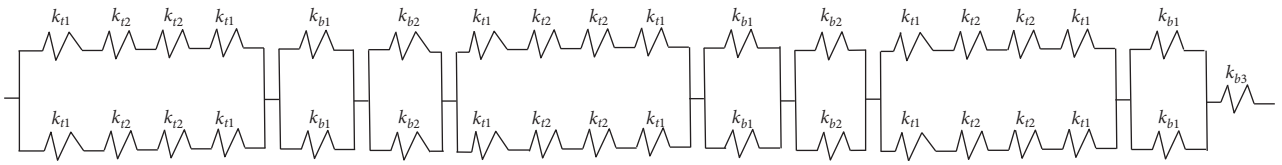

Figure 3: Stiffness plot of basic LET.

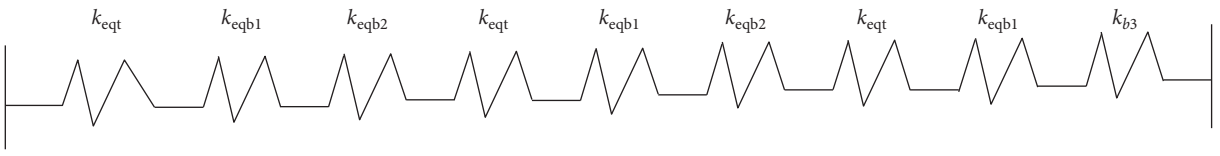

Figure 4: Stiffness plot of basic LET.

$$G = \frac{E}{2(1+\nu)}, \tag{10}$$

in which modulus of rigidity is G and Poisson's ratio is ν. Other parameters such as (w_{t1}, L_{t1}) and (w_{t2}, L_{t2}) are the width and thickness of segment, respectively.

As the aforementioned design (see in Figure 3), the FHA includes three LETs being connected in a series through the bending element k_{b3} (see in Figure 5). The stiffness of system (I) is assumed as K_I, one of the second system II is K_{II}, and one of the third one is K_{III} (see in Figure 2).

The stiffness of springs system (I) is similar to the equivalent stiffness of torsional elements and yielded as

$$K_I = K_{\text{eq–basic LET}}, \tag{11}$$

in which K_I represents the equivalent stiffness of the springs systems (I).

Overall stiffness of the flexure hinge array is determined as

$$\frac{1}{K_{\text{eq–FHA}}} = \frac{1}{K_I} + \frac{1}{k_{b3}} + \frac{1}{K_{II}} + \frac{1}{k_{b3}} + \frac{1}{K_{III}}, \tag{12}$$

in which $K_{\text{eq-FHA}}$ is the stiffness of the flexure hinge array.

Displacement (Δ) versus load (F) of the flexure hinge array is assumed by

$$\Delta = \frac{F}{K_{\text{eq–FHA}}}. \tag{13}$$

4. Results and Discussion

4.1. Simulations. The purpose of deformation analysis is to consider the maximum range of displacement and load in which the FHA can withstand to ensure reliability in operation.

Stainless steel, ABS, PE, and AL are potential materials of the FHA (see in Table 2). Simulations are performed in ANSYS 18.1 software. Several common ways to mesh the model with irregular shapes are, e.g., sweep, map meshing, and face meshing. In this study, the model is meshed by face method. The model is meshed again. The meshed model has relatively good convergence with Skewness index of 0.5495. The nodes are 171211 nodes and the elements are 80599 elements (see in Figure 6).

By using the FHA made of stainless steel, it can supper a maximum force of 10 N in the x-direction. It can reach a maximum displacement of 1.84 mm. The stress is about 193.29 MPa. A similar analysis is implemented for the FHA made of ABS; it can achieve a maximum displacement of 30.85 mm under a force of 2 N with stress of 38.5 MPa. Next, the FHA is made of PE; it can move a maximum displacement of 32.33 mm under a force of 1 N with stress of 19.33 MPa. Meanwhile, the FHA is made of AL; it can reach a displacement of 12.39 mm with maximum force of 25 N and stress 481.81 MPa (see in Table 2).

The FHA with almost materials is in safety area of elastic limitation. However, the FHA with aluminum permits the best displacement with a max force of 25 N. When increasing the force over 30 N, the FHA is over elastic area of material due to the max stress (σ_m of 578, 18 MPa) over a limited stress (σ_l of 503 MPa).

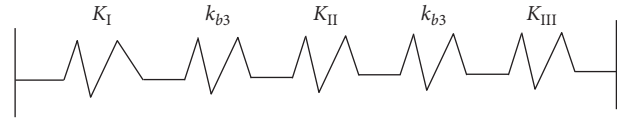

Figure 5: Stiffness diagram of the flexure hinge array.

4.2. Optimization of Displacement. It is noted that if the x-displacement is increased, the corresponding z-displacement is raised as well. Therefore, the x-displacement is considered as the cost function to be maximized. The goal of the optimization process is to improve the displacement of the FHA. In Figure 1(b), there are three important parameters which are considered as design variables, including L_{t1}, w_{t1}, and w_{t2} while the remaining parameters of the FHA are constant. The influences of those three parameters on the displacement are analyzed in Figure 7. These influences have a nonlinear sensitivity.

Recently, a metaheuristic algorithm is often adopted to enhance the quality or specification of a product. For instance, particle swarm optimization (PSO) and genetic algorithm (GA) were combined with artificial neural network to predict the pile bearing capacity [37]. Multiobjective genetic algorithm was applied to optimize the thermal process of battery [38] and NSGA-II was used to optimize the optimization design of battery [39]. A design optimization was implemented by ANSYS workbench to optimize operation parameters of a photovoltaic thermal system integrated with natural zeolite [40]. Adaptive neuro-fuzzy technique was applied to optimize the crystal growing of carbon nanotubes [41]. A neural saliency algorithm was devoted to recognize a perception style transfer [42]. A dice similarity measure was based on complex neutrosophic to recognize the pattern model [43]. A dual local search-based multiobjective optimization was developed to optimize a hyperchaotic map and image encryption [44]. Additionally, a 7-D hyperchaotic map was suggested for an image encryption [45]. On the contrary, in this paper, moth-flame optimization (MFO) algorithm is utilized to solve the optimization problem of the FHA, thanks to its efficiency and simplification. The flowchart of this algorithm is shown as in Figure 8(a). Details of the MFO can be found in the literature [35, 46]. A pseudocode for the MFO is given, as shown in Figure 8(b).

The optimization process is programmed in MATLAB R2019b; the optimal parameters are found at L_{t1} of 20.58 mm, w_{t1} of 1.92 mm, and w_{t2} of 2.29 mm. Finally, the optimal displacement is found approximately 27.02 mm.

A comparison of the MFO with common algorithms (GA, PSO, and DE) is conducted by a nonparameter statistical method, Kruskal–Wallis test [47]. In order to a fair comparison, each algorithm is run with an initial population of 20 and a maximum iteration of 500. Besides, each method is implemented 35 times in MATLAB R2019b. The

Table 2: Results of displacement of the flexure hinge array.

Material	Yield strength, σ_l (MPa)	Young's modulus (MPa)	Max force (N)	Max stress, σ_m (MPa)	Max displacement (mm)	Comparison
Stainless steel	207	193000	10	193.29	1.84	$\sigma_l > \sigma_m$
ABS	43.6	2300	2	38.5	30.85	$\sigma_l > \sigma_m$
PE	25	1100	1	19.33	32.23	$\sigma_l > \sigma_m$
Al	503	71700	25	481.81	12.39	$\sigma_l > \sigma_m$

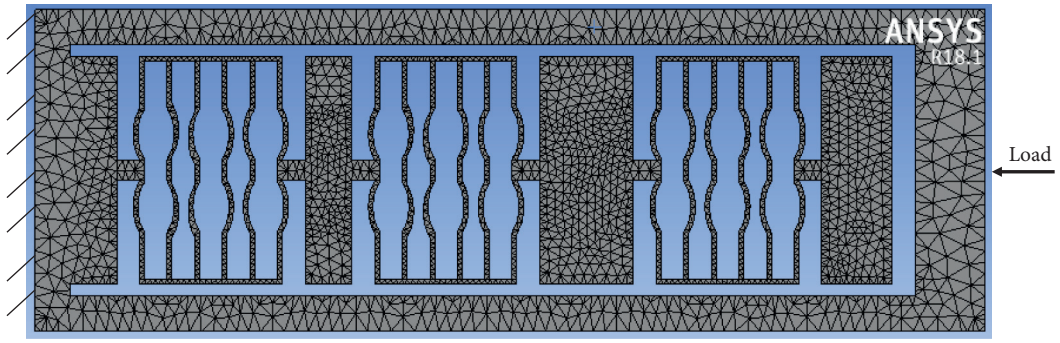

Figure 6: Meshed model of flexure hinge array.

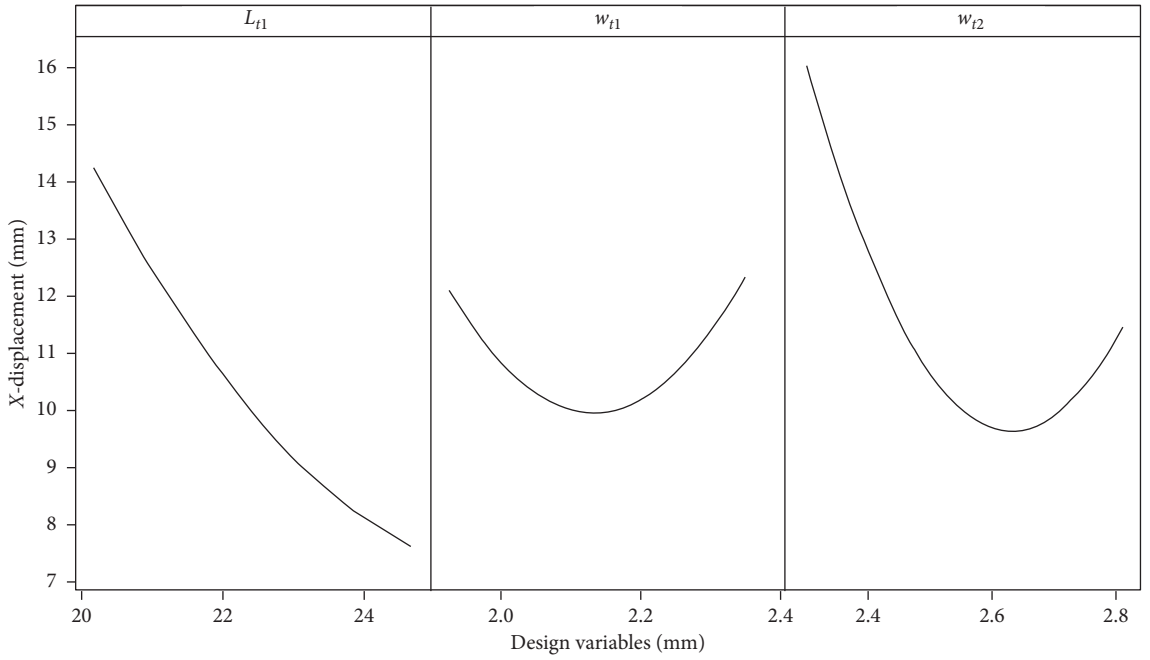

Figure 7: Sensitivity plot of design variables to the displacement.

results found that there is statistical difference among the MFO and three other algorithms. It showed that the MFO outperforms the other methods in finding the best displacement for the FHA with p value smaller than 0.001, as given in Table 3.

4.3. Experiments. Through aforementioned simulations and analyses, Al material is suitable for the proposed FHA. A prototype of basic LET and a prototype of FHA are made by Al, as given in Figure 9.

A force from a force gauge is acted to free end of the FHA; the FHA moves in the horizontal direction. At the same time, the FHA emerges the z-direction (see in Figures 10 and 11).

4.4. Comparison between Theory and Experiment. In this section, validity for theoretical models is verified by simulations and experiment. A prototype of the FHA is made of Al material. Boundary conditions include a fixed end and a free end is acted by a load of 25 N. The errors between the computation

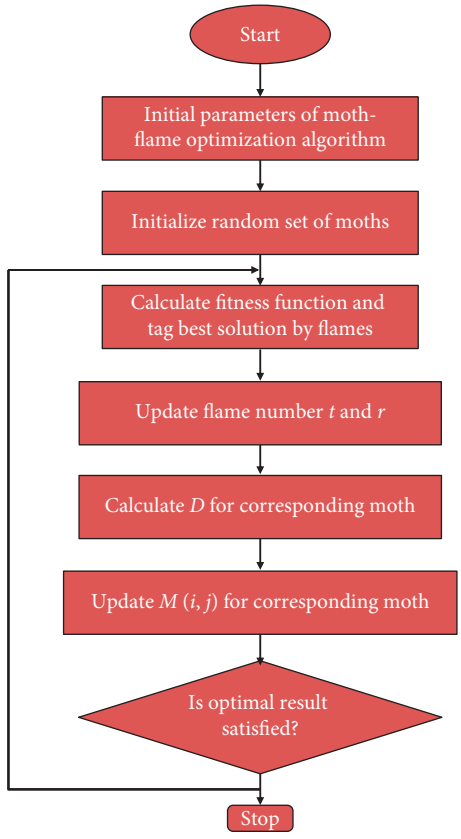

(a)

Pseudocode of the MFO:

Initialize the moth-flame parameters
Randomly initialize the moth position
for i = 1 to n do
  compute the cost function
end for
while iteration ≤ max iterations do
  update the moth position
  compute the flames' number
  evaluate the cost function
  if iteration == 1 then
    F = sort (M) and OF = sort (OM)
  else
    F = sort (M_{t-1}, M_t) and OF = sort (M_{t-1}, M_t)
  else if
  for i = 1 to n do
    for j = 1 to d do
      update the values of r and t
      compute the values of D with respect to the corresponding moth
      update $M(i, j)$ with respect to the corresponding moth
    end for
  end for
end while
Print the best values

(b)

Figure 8: The MFO. (a) Flowchart; (b) pseudocode.

Table 3: Kruskal–Wallis test: MFO versus other algorithms.

Algorithms	Number of runs	Median displacement	Mean rank	Z value
DE	35	26.89	53.0	−2.95
GA	35	26.85	18.0	−8.84
MFO	35	27.02	123.0	8.84
PSO	35	26.92	88.0	2.95
Overall	140		70.5	
H value	130.32			
p value	<0.001			

and simulation (E_c) and errors among the theoretical computation and the experiment (E_e) are calculated.

$$E_c = \frac{\left|\Delta_{\text{simulation}} - \Delta_{\text{theory}}\right|}{\Delta_{\text{simulation}}} * 100, \tag{14}$$

$$E_e = \frac{\left|\Delta_{\text{experiment}} - \Delta_{\text{theory}}\right|}{\Delta_{\text{experiment}}} * 100. \tag{15}$$

As given in Table 4, it finds that E_c is about 5.66% while E_e is around 7.11%. It verifies that the analytical models are relatively good.

4.5. Comparison of the Proposed Hinge with the Existing Joints. In conforming the behaviors of the FHA, another LET_C (common LET hinge) with its shape in Figure 12 is made. The experimental results are then treated as the normalized values for comparison among different types of hinges. Normalization is determined by

$$\overline{y}_i = \frac{y_i - y_{\min}}{y_{\max} - y_{\min}}, \tag{16}$$

in which $\overline{y}_i$ is the normalized value and y_i, $y_{\min}$, and $y_{\max}$ are the ith raw value, minimum value, and maximum value, respectively.

Among the three types, the displacement of the FHA is the highest (see in Figure 13).

Figure 14 illustrates a relation between the x-displacement and the z-displacement of the FHA. It finds that the FHA can reach a max displacement of 32.3 mm in the z-direction.

A relationship of driving force in x-direction and displacement in z-direction is provided, as shown in Figure 15.

4.6. Buckling Analysis. Buckling is a popularly unstable failure of a rigid structure. The structures are designed to avoid this phenomenon. In this study, the structure FHA is desired to reach a large displacement in the z-direction when applying a load in the x-direction. When discovering the buckling phenomenon of the FHA, it finds that the FHA is easy to lead to buckling if the eigen value is low. If the eigen value is small, the FHA is easy to make a large displacement

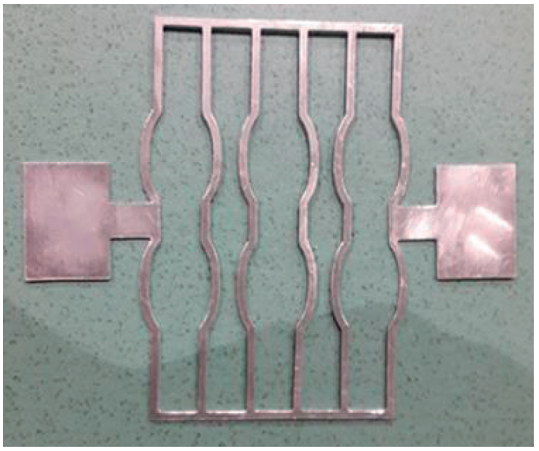

(a)

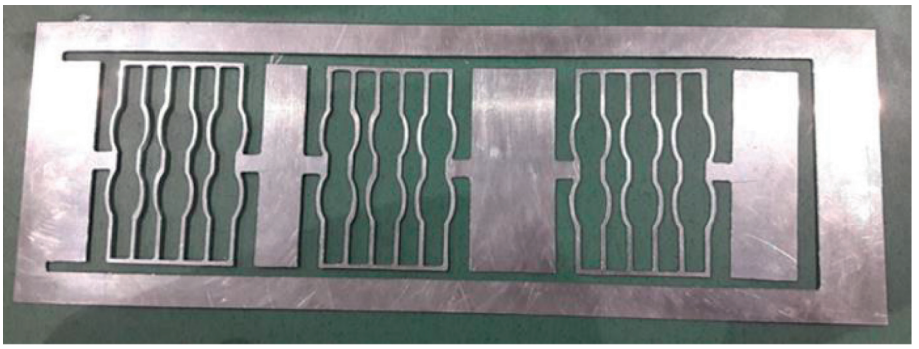

(b)

Figure 9: Prototype: (a) LET; (b) flexure hinge array.

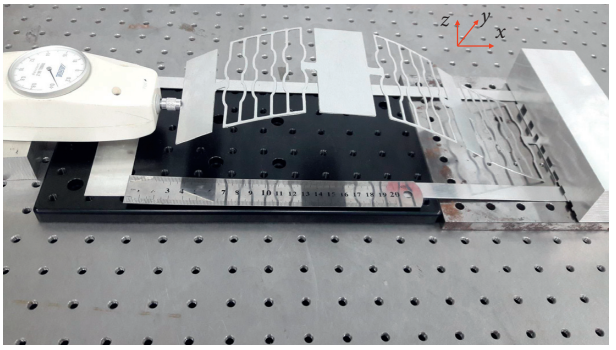

Figure 10: Deformation of flexure hinge array in the x-direction.

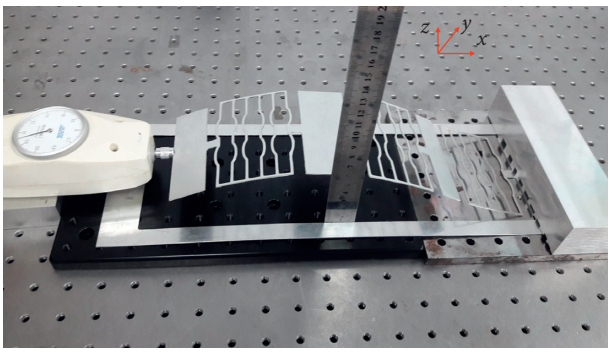

Figure 11: Deformation of flexure hinge array in the z-direction.

Table 4: Comparison results.

Force (N)	5	10	15	20	25
Δ-theory (mm)	2.61	5.23	7.85	10.47	13.10
Δ-simulation (mm)	2.47	4.95	7.43	9.91	12.39
Δ-experiment (mm)	2.81	5.64	8.47	11.29	14.12
E_c (%)			5.66		
E_e (%)			7.11		

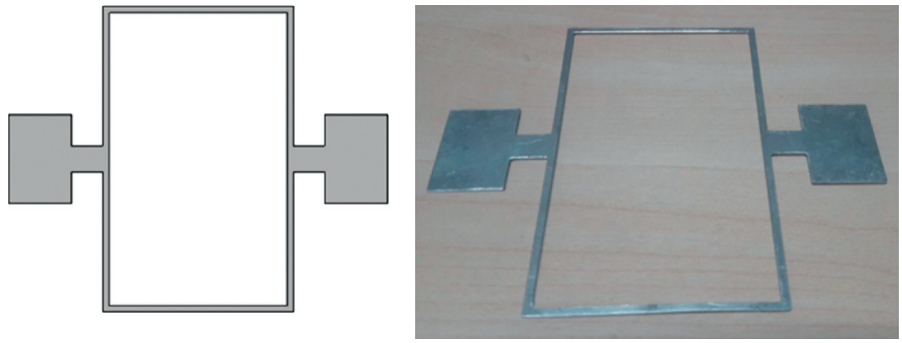

(a) (b)

Figure 12: A LET_C: (a) 2D CAD; (b) prototype.

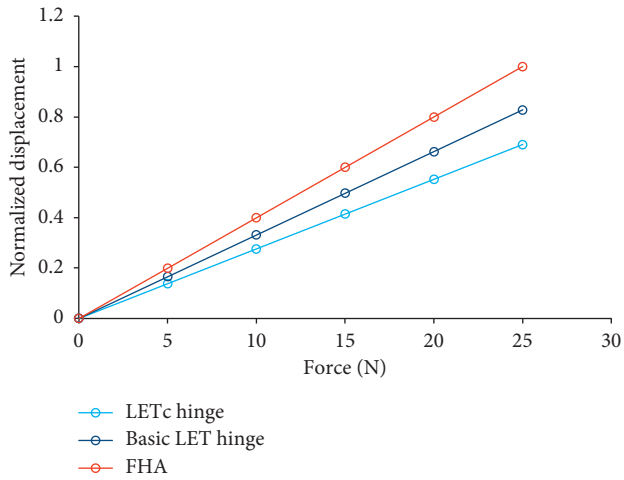

Figure 13: Comparison of displacement.

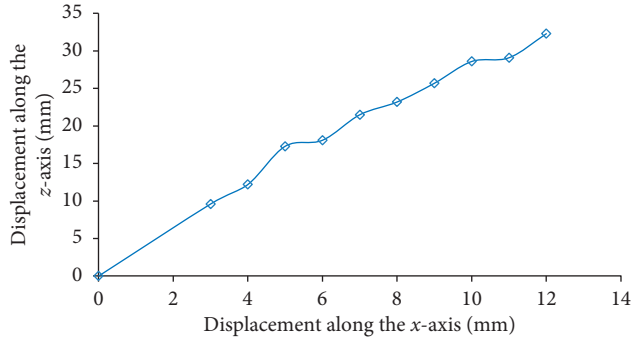

Figure 14: Diagram of x-displacement vs z-displacement of the flexure hinge array.

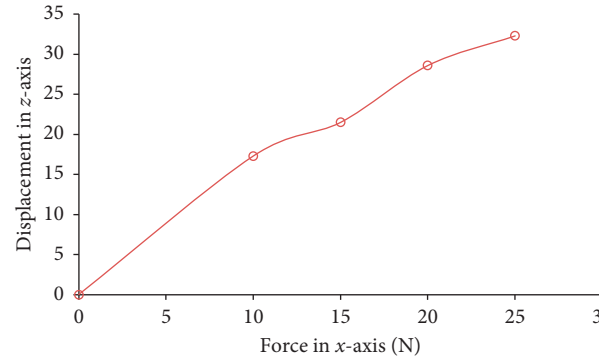

Figure 15: Relationship of driving force in x-direction vs displacement in z-direction.

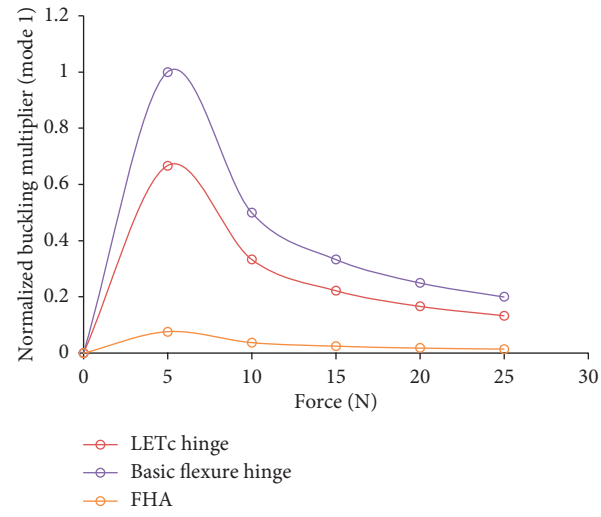

Figure 16: Comparison of buckling behavior.

in the z-direction. In the other word, the buckling may be another advantage of the FHA. Considering the buckling of a cantilever beam, critical load (f) can be determined [48]:

$$f = \frac{EI\pi^2}{4L^2}, \tag{17}$$

in which Young's modulus is E, second moment of area is I, and length is L.

On the contrary, simplified equation is as follows:

$$P_c = \lambda \times P_I, \quad \text{where } \lambda \text{ is the eigen value or multiplier load and } P_I \text{ is the unit load.} \tag{18}$$

A range of loads from 5 N to 25 N is applied to the FHA in the x-direction to reach the eigen value. The simulated results find that the eigen value of the suggested FHA is the lowest (see in Figure 16). This means that the FHA is easy to deform in both x- and z-directions.

5. Conclusions

This article presented a new design of flexure hinge array. In this paper, a few TLET hinges were connected in series to create a new FHA. The proposed FHA was capable of providing a large displacement in the desired motion directions. The theoretical equations for understanding the stiffness and displacement of the proposed FHA were deduced. Furthermore, the static modeling of the FHA was given. In order to enhance the displacement of the FHA, the MFO was applied to search the best parameters for designing the FHA.

The results found that the optimal displacement is about 27.02 mm along the x-axis. The results indicated that optimal parameters include L_{t1} of 20.58 mm, w_{t1} of 1.92 mm, and w_{t2} of 2.29 mm. The optimal displacement is approximately 27.02 mm. In addition, the performance of the MFO was compared with that of the GA, PSO, and DE. By using the Kruskal–Wallis test, the results indicated that the behavior of MFO is more effective than that of three other algorithms in terms of finding the best displacement for the proposed FHA. Besides, the results showed that the errors among the prediction and verification are around from 5% to 7%. It verified that the analytical equations are relatively suitable to demonstrate the static characterizations of the FHA.

In selecting a suitable material, the Al material was chosen for fabricating the FHA in comparison with stainless steel, ABS, and PE. Furthermore, the result determined that the FHA can reach a large displacement of 12 mm with a max force of 25 N. Additionally, the displacement and buckling value of FHA were better than those of other hinges. It also found that the FHA can achieve the z-displacement of 32.3 mm. In future work, other specifications of the FHA will be studied. Then, a real application of the FHA will be considered.

Data Availability

Data used to support the findings of this study are included within the article.

Conflicts of Interest

The authors declare that there are no conflicts of interest regarding the publication of this article.

Acknowledgments

This research was funded by the Vietnam National Foundation for Science and Technology Development (NAFOSTED) under Grant no. 107.01-2019.14.

References

[1] M. Ling, J. Cao, Z. Jiang, and Q. Li, "Development of a multistage compliant mechanism with new boundary constraint," *Review of Scientific Instruments*, vol. 89, 2018.

[2] D. N. Nguyen, T. Dao, N. Le Chau, and V. A. Dang, "Hybrid approach of finite element method , kigring metamodel , and multiobjective genetic algorithm for computational optimization of a flexure elbow joint for upper-limb assistive device," *Complexity*, vol. 2019, Article ID 3231914, 13 pages, 2019.

[3] N. T. Tran, N. Le Chau, and T. P. Dao, "A new butterfly-inspired compliant joint with 3-DOF in-plane motion," *Arabian Journal for Science and Engineering*, vol. 115 pages, 2020.

[4] G. Berselli, Q. Meng, R. Vertechy, and V. P. Castelli, "An improved design method for the dimensional synthesis of flexure-based compliant mechanisms: optimization procedure and experimental validation," *Meccanica*, vol. 51, pp. 1209–1225, 2016.

[5] Q. Meng, Y. Li, and J. Xu, "A novel analytical model for flexure-based proportion compliant mechanisms," *Precision Engineering*, vol. 38, no. 3, 2014.

[6] N. Linh and H. T. Dao, "Optimal design of a compliant micrograpper for assemble system of cell phone vibration motor using a hybrid approach of ANFIS and jaya," *Arabian Journal for Science and Engineering*, vol. 44, pp. 1205–1220, 2018.

[7] M. Ling, J. Cao, Z. Jiang, and J. Lin, "A semi-analytical modeling method for the static and dynamic analysis of complex compliant mechanism," *Precision Engineering*, vol. 52, pp. 64–72, 2018.

[8] Y. Du, T. Li, and G. Gao, "Dynamic analysis of a flexure-based compliant stage," *Journal of Mechanical Science and Technology*, vol. 32, pp. 5223–5231, 2018.

[9] T.-P. Dao, S.-C. Huang, and N. Le Chau, "Robust parameter design for a compliant micrograpper based on hybrid Taguchi-differential evolution algorithm," *Microsystem Technologies*, vol. 24, no. 6, pp. 1–17, 2017.

[10] N. Le Chau, N. T. Tran, and T. P. Dao, "A multi-response optimal design of bistable compliant mechanism using

efficient approach of desirability, fuzzy logic, ANFIS and LAPO algorithm," *Applied Soft Computing*, vol. 94, Article ID 106486, 2020.

[11] N. Le Chau, H. G. Le, T.-P. Dao, and V. A. Dang, "Design and optimization for a new compliant planar spring of upper limb assistive device using hybrid approach of RSM–FEM and MOGA," *Arabian Journal for Science and Engineering*, vol. 44, pp. 7441–7456, 2019.

[12] E. G. Merriam and L. L. Howell, "Non-dimensional approach for static balancing of rotational fl exures," *Manitoba Association of Mathematics Teachers*, vol. 84, 2015.

[13] Y. K. Yong, S. S. Aphale, and S. O. R. Moheimani, "Design, identification, and control of a flexure-based XY stage for fast nanoscale positioning," *IEEE Transactions on Nanotechnology*, vol. 8, pp. 46–54, 2009.

[14] T. P. Dao and S. C. Huang, "Design and multi-objective optimization for a broad self-amplified 2-DOF monolithic mechanism," *Academy Proceedings in Engineering Science*, vol. 42, pp. 1527–1542, 2017.

[15] G. Hao, X. He, and S. Awtar, "Design and analytical model of a compact flexure mechanism for translational motion," *Mechanism and Machine Theory*, vol. 142, 2019.

[16] N. L. Ho, T. Dao, H. G. Le, and N. Le Chau, "Optimal design of a compliant microgripper for assemble system of cell phone vibration motor using a hybrid approach of ANFIS and jaya," *Arabian Journal for Science and Engineering*, vol. 44, pp. 1205–1220, 2019.

[17] J. O. Jacobsen, B. G. Winder, L. L. Howell, and S. P. Magleby, "Lamina emergent mechanisms and their basic elements," *Journal of Mechanisms and Robotics*, vol. 2, pp. 1–9, 2010.

[18] I. L. Delimont, "Compliant joints suitable for use as surrogate folds," 2014.

[19] J. O. Jacobsen and S. P. Magleby, "Fundamental for the design of lamina emergent mechanisms," 2016.

[20] P. S. Gollnick, S. P. Magleby, and L. L. Howell, "An introduction to multilayer lamina emergent mechanisms," *The ASME Journal of Mechanical Design*, vol. 133, 2011.

[21] Z. Xie, L. Qiu, and D. Yang, "Design and analysis of a variable stiffness inside-deployed lamina emergent joint," *Mechanism and Machine Theory*, vol. 120, pp. 166–177, 2018.

[22] Z. Xie, L. Qiu, and D. Yang, "Design and analysis of outside-deployed lamina emergent joint (OD-LEJ)," *Mechanism and Machine Theory*, vol. 114, pp. 111–124, 2017.

[23] J. O. Jacobsen, G. Chen, L. L. Howell, and S. P. Magleby, "Lamina emergent torsional (LET) joint," *Mechanism and Machine Theory*, vol. 44, pp. 2098–2109, 2009.

[24] S. E. Wilding, L. L. Howell, and S. P. Magleby, "Introduction of planar compliant joints designed for combined bending and axial loading conditions in lamina emergent mechanisms," *Mechanism and Machine Theory*, vol. 56, pp. 1–15, 2012.

[25] G. Information, "Lamina emergent torsion joints," 2009.

[26] H. C. Greenberg, *Using Lamina Emergent Mechanisms to Address Needs for a Space Environment*, Brigham Young University, Provo, Utah, 2011.

[27] S. E. Wilding, L. L. Howell, and S. P. Magleby, "Spherical lamina emergent mechanisms," *Mechanism and Machine Theory*, vol. 49, pp. 187–197, 2012.

[28] R. Alfattani and C. Lusk, "A lamina-emergent frustum using a bistable collapsible compliant mechanism," *The ASME Journal of Mechanical Design*, vol. 140, pp. 1–9, 2018.

[29] G. Chen, S. P. Magleby, and L. L. Howell, "Membrane-enhanced lamina emergent torsional joints for surrogate folds," *The ASME Journal of Mechanical Design*, vol. 140, pp. 1–10, 2018.

[30] X. Sun and B. Yang, "Sensors and actuators a : physical a new methodology for developing flexure-hinged displacement amplifiers with micro-vibration suppression for a giant magnetostrictive micro drive system," *Sensors and Actuators A: Physical*, vol. 263, 2017.

[31] H. Zhang, X. Zhang, and B. Zhu, "A novel flexural lamina emergent spatial joint," *Mechanism and Machine Theory*, vol. 142, Article ID 103582, 2019.

[32] W. Le Zhu, Z. Zhu, P. Guo, and B. F. Ju, "A novel hybrid actuation mechanism based XY nanopositioning stage with totally decoupled kinematics," *Mechanical Systems and Signal Processing*, vol. 99, pp. 747–759, 2018.

[33] N. Thoai, T. Ngoc, and L. Chau, "A new butterfly-inspired compliant joint with 3-DOF in-plane motion," *Arabian Journal for Science and Engineering*, vol. 1, 2020.

[34] D. B. Ferrell, Y. F. Isaac, S. P. Magleby, and L. L. Howell, "Development of criteria for lamina emergent mechanism flexures with specific application to metals," *The Journal of Mechanical Design*, vol. 133, pp. 1–9, 2011.

[35] M. P. Dang, H. G. Le, N. Le Chau, and T. Dao, "Optimization for a flexure hinge using an effective hybrid approach of fuzzy logic and moth-flame optimization algorithm," *Mathematical Problems in Engineering*, vol. 2021, Article ID 6622655, 18 pages, 2021.

[36] R. J. Roark, W. C. Young, and R. Plunkett, "Formulas for stress and strain," *The Journal of Applied Mechanics*, vol. 43, no. 3, p. 522, 1976.

[37] B. R. Murlidhar, R. K. Sinha, E. T. Mohamad, R. Sonkar, and M. Khorami, "The effects of particle swarm optimisation and genetic algorithm on ANN results in predicting pile bearing capacity," *International Journal of Hydromechatronics*, vol. 3, no. 1, 2020.

[38] W. Li, M. Xiao, X. Peng, A. Garg, and L. Gao, "A surrogate thermal modeling and parametric optimization of battery pack with air cooling for EVs," *Applied Thermal Engineering*, vol. 147, no. 5, p. 1, 2019.

[39] Y. Zhang, S. Chen, M. E. Shahin et al., "Multi-objective optimization of lithium-ion battery pack casing for electric vehicles: key role of materials design and their influence," *International Journal of Energy Research*, vol. 44, no. 3, 2020.

[40] C. Kandilli and B. Mertoglu, "Optimisation design and operation parameters of a photovoltaic thermal system integrated with natural zeolite," *International Journal of Hydromechatronics*, vol. 3, no. 2, pp. 128–139, 2020.

[41] M. Safa, M. Ahmadi, J. Mehrmashadi et al., "Selection of the most influential parameters on vectorial crystal growth of highly oriented vertically aligned carbon nanotubes by adaptive neuro-fuzzy technique," *International Journal of Hydromechatronics*, vol. 3, no. 3, 2020.

[42] C. Zhu, W. Yan, X. Cai, S. Liu, T. H. Li, and G. Li, "Neural saliency algorithm guide bi-directional visual perception style transfer," *CAAI Transactions on Intelligence Technology*, vol. 5, no. 1, 3 pages, 2020.

[43] Z. Ali and T. Mahmood, "Complex neutrosophic generalised dice similarity measures and their application to decision making," *CAAI Transactions on Intelligence Technology*, vol. 5, no. 2, pp. 78–87, 2020.

[44] M. Kaur and D. Singh, "Multiobjective evolutionary optimization techniques based hyperchaotic map and their applications in image encryption," *Multidimensional Systems and Signal Processing*, vol. 32, no. 1, 2021.

[45] M. Kaur, D. Singh, and V. Kumar, "Color image encryption using minimax differential evolution-based 7D hyper-chaotic map," *Applied Physics B: Lasers & Optics*, vol. 126, 2020.
[46] M. Shehab, L. Abualigah, H. Al Hamad, H. Alabool, M. Alshinwan, and A. M. Khasawneh, "Moth–flame optimization algorithm: variants and applications," *Neural Computing and Applications*, vol. 32, no. 11, pp. 1–26, 2020.
[47] G. Y. Zhu and W. B. Zhang, "Optimal foraging algorithm for global optimization," *Applied Soft Computing*, vol. 51, pp. 294–313, 2017.
[48] T.-P. Dao and S.-C. Huang, "Compliant thin-walled joint based on zygoptera nonlinear geometry," *Journal of Mechanical Science and Technology*, vol. 31, 2017.